CONF-890842

APPLICATIONS OF ADINA TO VISCOPLASTIC-DYNAMIC FRACTURE MECHANICS ANALYSIS

B. R. Bass
J. Keeney-Walker
T. L. Dickson
C. E. Pugh
Oak Ridge National Laboratory
Oak Ridge, Tennessee

C. W. Schwartz
University of Maryland
College Park, Maryland

J. C. Thesken
Royal Institute of Technology
Stockholm, Sweden

CONF-890842--1

DE89 006624

APPLICATIONS OF ADINA TO VISCOPLASTIC-DYNAMIC FRACTURE MECHANICS ANALYSIS*

B. R. Bass
J. Keeney-Walker
T. L. Dickson
C. E. Pugh
Oak Ridge National Laboratory
Oak Ridge, Tennessee

C. W. Schwartz
University of Maryland
College Park, Maryland

J. C. Thesken
Royal Institute of Technology
Stockholm, Sweden

Abstract — Nonlinear rate-dependent effects in crack run-arrest events in ductile materials are being investigated through development and applications of viscoplastic-dynamic finite element analysis techniques. This paper describes a portion of these studies wherein various viscoplastic constitutive models, dynamic crack-propagation algorithms, and proposed nonlinear fracture criteria have been installed in the general purpose ADINA finite element computer program. The predictive capabilities of the nonlinear techniques are evaluated through analyses of crack-arrest tests of nonisothermal wide-plate specimens. Values of fracture parameters calculated by elastodynamic and viscoplastic dynamic techniques are compared to assess the impact of including

*Research sponsored by the Office of Nuclear Regulatory Research, U.S. Nuclear Regulatory Commission under Interagency Agreements 1886-8011-9B with the U.S. Department of Energy under Contract DE-AC05-840R21400 with Martin Marietta Energy systems, Inc.

viscoplastic effects in the computational models. Mesh refinement studies are presented that examine whether the proposed fracture parameters converge to nonzero values in viscoplastic dynamic analyses or whether they are controlled by element dimensions. Plans are reviewed for additional computational studies to assess the utility of viscoplastic analysis techniques in constructing a dynamic inelastic fracture mechanics model for ductile steels.

1. INTRODUCTION

In pressurized-thermal-shock (PTS) scenarios, inner surface cracks of reactor pressure vessels (RPVs) have the greatest propensity to propagate because they are located in the region of highest thermal stress, lowest temperature and greatest irradiation damage. If such a crack begins to propagate radially through the vessel wall, it will extend into a region of higher fracture toughness due to the higher temperatures and less irradiation damage. The Heavy-Section Steel Technology (HSST) Program at the Oak Ridge National Laboratory (ORNL) under the sponsorship of the Nuclear Regulatory Commission (NRC) is conducting experimental and analytical studies aimed at the circumstances that would initiate the growth of an existing crack in an RPV and the conditions that can lead to the arrest of a propagating crack.

Fracture models used in these integrity assessments are developed in part from small-specimen crack-arrest data that can include significant dynamic effects (e.g., stress waves reflected back to the running crack tip). Prior studies of crack arrest have focused on reducing these dynamic effects and on developing dynamic analysis capabilities

for interpreting small-specimen data. Small specimens, however, provide limited constraint of deformation in the crack-plane region and permit only the generation of data at temperatures below those where arrest is likely to occur in some PTS scenarios. Recently, the HSST program has generated crack-arrest data over an expanded temperature range through tests of large wide-plate specimens [1—3]. This paper addresses the development of computational analysis methods incorporating nonlinear and dynamic effects for interpreting crack run-arrest behavior in these ductile materials.

Two viscoplastic constitutive models and several proposed nonlinear fracture criteria have been installed in the ADINA [4] finite element program at ORNL. An effective-stress algorithm described by Kojić and Bathe [5] is used to integrate the constitutive equations. The capabilities of these nonlinear techniques for modeling dynamic fracture events in ductile RPV steels are illustrated for one of the HSST wide-plate crack-arrest experiments [1]. Mesh refinement studies are summarized that examine the dependence of the proposed fracture parameters on element dimensions within the crack-tip region. Finally, alternative fracture parameters and computational techniques selected to circumvent stringent requirements on crack-tip mesh refinement in inelastic analyses are reviewed.

2. IMPLEMENTATION OF A VISCOPLASTIC CONSTITUTIVE FORMULATION

Until recently, linear elastic fracture mechanics (LEFM) concepts have been dominant in applications of dynamic analysis techniques to crack-arrest studies (e.g., Ref. 2). However, except for very short crack jumps, LEFM assumptions may not be valid characterizations of

rapid crack propagation [6]. In particular, a wake of residual plasticity left behind the moving crack tip can violate the K_I - dominance requirement of LEFM. An indication that LEFM conditions are not satisfied occurs when elastodynamic analyses of crack run-arrest data lead to geometry-dependent fracture toughness relations (e.g., Ref. 7). Dahlberg et al. [7] performed elastodynamic fracture analyses using crack run-arrest data from tests of single-edge-notched (SEN) tension panel specimens of different lengths. Their results for different panel lengths coincide for low crack velocities, but show a definite geometry dependence at higher velocities where strain-rate effects are more pronounced. However, Brickstad [8] has demonstrated that this geometry dependence can be removed through application of an inelastic fracture model that incorporates plasticity and strain-rate effects (i.e., viscoplasticity).

These studies indicate that strain-rate effects ($\sim 10^4$ sec^{-1}) can be important for rapid-loading situations such as cleavage crack propagation events in ductile RPV steels. The HSST Program research efforts at ORNL and several subcontracting groups are developing viscoplastic-dynamic finite element analysis techniques and validating their utility through the analysis of data from carefully performed crack-arrest experiments [9]. The first two viscoplastic constitutive models selected for examination were the Bodner-Partom [10] model with strain-hardening and a variation of the Perzyna [11] model with linear strain-hardening. The functional forms of these viscoplastic models implemented in ADINA are summarized below.

2.1 Bodner-Partom Constitutive Model

The implementation of the Bodner-Partom [10] viscoplastic model in ADINA is based on the formulation described by Kanninen et al. [12] and is summarized in Table 1. Kanninen et al. [12] obtained and used dynamic stress-strain data from tensile and split — Hopkinson bar tests to derive constants for the Bodner-Partom constitutive model appropriate for A533 grade B class 1 (A533B) steel at the test temperatures listed in Table 2. Dynamic stress-strain curves computed by the Bodner-Partom model at temperature T = 100°C and strain rates 550 s^{-1} and 0.001 s^{-1} are compared with measured data in Fig. 1. Temperature dependence of the material properties is taken into account principally through the dependence of n, Z_0 and Z_1 on temperatures as indicated in Table 2.

2.2 Perzyna Constitutive Model

The viscoplastic model of Perzyna [11] has been implemented in finite element formulations by Thakkar and Stagg [13] and used in dynamic crack-propagation studies by Brickstad [8]. The Perzyna formulation adopted for the HSST studies is based on the von Mises yield criterion with linear strain hardening and is summarized in Table 3. Material parameters for the Perzyna constitutive model (Table 4) were developed by Brickstad [14] using the same dynamic stress-strain data for A533B steel obtained by Kanninen et al. [12].

2.3 Finite Element Formulation of the Viscoplatic Solution Algorithm

The viscoplastic formulations of Tables 1-4 were installed in ADINA at ORNL through modification of the thermo-elastoplastic and creep model (material model 10) employed in ADINA and described by Kojić and Bathe

[5]. The modified formulation of equilibrium and constitutive equations can be expressed in vector form at time t + Δt as

$$\int_V \underline{B}^T \, {}^{t+\Delta t}\underline{\sigma} \, dV = {}^{t+\Delta t}\underline{R} \, , \tag{1}$$

$${}^{t+\Delta t}\underline{S} = \frac{{}^{t+\Delta t}E}{1+{}^{t+\Delta t}\nu} \left({}^{t+\Delta t}\underline{e}'' - \Delta \underline{e}^P \right) , \tag{2}$$

$${}^{t+\Delta t}\underline{e}'' = {}^{t+\Delta t}\underline{e}' - {}^{t}\underline{e}^P \tag{3}$$

$${}^{t+\Delta t}\sigma_m = \frac{{}^{t+\Delta t}E}{1-2{}^{t+\Delta t}\nu} \left({}^{t+\Delta t}e_m - {}^{t+\Delta t}e^{th} \right) \tag{4}$$

where for time t + Δt

$\underline{B}$ = the total strain-displacement transformation matrix,

${}^{t+\Delta t}\underline{\sigma}$ = the stress tensor,

${}^{t+\Delta t}\underline{R}$ = the nodal point external load vector,

${}^{t+\Delta t}\underline{S}$ = deviatoric stress tensor,

$= {}^{t+\Delta t}\sigma_{ij} - {}^{t+\Delta t}\sigma_m \, \delta_{ij}$,

${}^{t+\Delta t}\underline{e}'$ = deviatoric strain tensor,

$= {}^{t+\Delta t}e_{ij} - {}^{t+\Delta t}e_m \, \delta_{ij}$

$^{t+\Delta t}\underline{e}^P$ = viscoplastic strain tensor,

$^{t+\Delta t}\sigma_m$ = mean stress = $^{t+\Delta t}\sigma_{ii}/3$,

$^{t+\Delta t}e_m$ = mean strain = $^{t+\Delta t}e_{ii}/3$,

$^{t+\Delta t}E$, $^{t+\Delta t}\nu$ = Young's modulus and Poisson's ratio corresponding to temperature $^{t+\Delta t}\theta$,

$^{t+\Delta t}e^{th}$ = thermal strain,

= $^{t+\Delta t}\alpha_m$ $(^{t+\Delta t}\theta - \theta_{ref})$,

$^{t+\Delta t}\alpha_m$ = mean coefficient of thermal expansion,

θ_{ref} = reference temperature

Assuming that solution variables are known at time t, the viscoplastic strain increment is determined using the α-method [5] and the formulation given by

$$\Delta\underline{e}^P = \Delta t\,{}^{\tau}\dot{\underline{e}}^P \tag{5}$$

where

$${}^{\tau}\dot{\underline{e}}^P = {}^{\tau}\gamma\,{}^{\tau}\underline{S}\ , \tag{6}$$

and

$${}^{\tau}\underline{S} = (1 - \alpha)\,{}^{t}\underline{S} + \alpha\,{}^{t+\Delta t}\underline{S}\ . \tag{7}$$

In Eq. (7), α is an integration parameter satisfying $0 \leq \alpha \leq 1$. The fully explicit and fully implicit integration schemes are represented

by $\alpha = 0$ and $\alpha = 1$, respectively. The functional form of the scalar ${}^{\tau}\gamma$ in Eq. (6) is determined by the choice of the viscoplastic constitutive model.

For the Bodner-Partom model of Table 1, the function ${}^{\tau}\gamma$ has the form

$$ {}^{\tau}\gamma = \frac{D_o}{{}^{\tau}J_2{}^{1/2}} \exp \left[- \frac{1}{2} \left(\frac{{}^{\tau}Z^2}{3\,{}^{\tau}J_2} \right)^{{}^{\tau}n} \right] \tag{8} $$

where

$$ {}^{\tau}Z = (1 - \alpha)\, {}^{t}Z + \alpha\, {}^{t+\Delta t}Z \,, \tag{9} $$

$$ {}^{t+\Delta t}Z = {}^{t+\Delta t}Z_1 + ({}^{t+\Delta t}Z_0 - {}^{t+\Delta t}Z_1) \exp\, (-m_1\, {}^{t+\Delta t}Wp) \,, \tag{10} $$

$$ {}^{\tau}J_2 = \frac{1}{2}\, {}^{\tau}S_{ij}\, {}^{\tau}S_{ij} \,, \tag{11} $$

and temperature dependent parameters are evaluated from

$$ {}^{\tau}\theta = (1 - \alpha)\, {}^{t}\theta + \alpha\, {}^{t+\Delta t}\theta \,. \tag{12} $$

The accumulated plastic work ${}^{t+\Delta t}Wp$ in Eq. (10) is determined from the relation

$$ {}^{t+\Delta t}Wp = {}^{t}Wp + \Delta Wp \,, \tag{13} $$

where

$$ \Delta Wp = {}^{\tau}\dot{W}p\, \Delta t = 2\, {}^{\tau}\gamma\, {}^{\tau}J_2\, \Delta t. \tag{14} $$

For the Perzyna model of Table 3, the function ${}^{\tau}\gamma$ has the form

$$ {}^{\tau}\gamma = \begin{cases} \beta\, {}^{\tau}\phi\, ({}^{\tau}\bar{\sigma})\, \frac{1}{2} \left(\frac{3}{{}^{\tau}J_2} \right)^{1/2} & \text{if } {}^{\tau}\bar{\sigma} > {}^{\tau}\bar{\sigma}_o \\ 0 & \text{if } {}^{\tau}\bar{\sigma} \leq {}^{\tau}\bar{\sigma}_o \end{cases} \tag{15} $$

where

$$\tau\phi(\tau\bar{\sigma}) = \left(\frac{\tau\bar{\sigma} - \tau\bar{\sigma}_o}{\tau\bar{\sigma}_o} \right)^N \tag{16}$$

$$\tau\bar{\sigma} = (3\ \tau J_2)^{1/2} , \tag{17}$$

$$\tau\bar{\sigma}_o = \sigma_{yI}(\tau\theta) + H'(\tau\theta)\ \tau\bar{e}^p , \tag{18}$$

$$\tau\bar{e}^p = (1 - \alpha)\ {}^t\bar{e}^p + \alpha\ {}^{t+\Delta t}\bar{e}^p , \tag{19}$$

and where the effective plastic strain is determined from

$$\bar{e}^p = \left(\frac{2}{3}\ e^p_{ij}\ e^p_{ij} \right)^{1/2} . \tag{20}$$

Equations (2) through (7) represent a one-parameter system of equations in the effective stress, ${}^{t+\Delta t}\bar{\sigma}$, which is obtained as the solution of the zero of the effective stress function $f({}^{t+\Delta t}\bar{\sigma})$ given by Eq. (2.32) of Ref. 5 with the rate-independent plasticity terms deleted. In ADINA, a bisection procedure with an acceleration scheme is used to solve the effective stress function for ${}^{t+\Delta t}\bar{\sigma}$, from which the updated stress tensor components are determined.

2.4 Numerical Example

The viscoplastic constitutive formulation implemented in the ORNL version of ADINA has been applied to a fixed-end beam subjected to a suddenly applied uniformly distributed load as depicted in Fig. 2. The problem was previously studied by Thakker and Stagg [13] and by

Brickstad [8] using the Perzyna model with a von Mises yield criterion, no strain hardening and a linear flow-rate function [i.e., $H' = 0$ in Eq. (18) and $N = 1$ in Eq. (16)]. Material and geometric parameters defining the problems are given as follows: Young's modulus $E = 68954.7$ MN/m^2, Poisson's ratio $\nu = 0.3$, density $\rho = 2672$ Kg/m^3, yield stress $\sigma_y = 276$ MN/m^2, length $L = 0.508$ m, height $h = 0.0254$ m, and distributed load $p_o = 43.78$ kN/m. The two-dimensional plane stress finite element model employed by Brickstad [8] was duplicated for the analyses of the present study. It consists of 200 four-noded bilinear element with ten elements through the thickness and utilizes symmetry to model one-half of the beam.

Dimensionless time histories for the central deflection of the beam are given in Fig. 2 for a range of values of the fluidity parameter, β. The static elastic deflection $\delta_o = 0.003174$ m (small deflection theory) and the period of the first natural mode $T_o = 0.00196028$ s were used to normalize the vertical and horizontal axes, respectively. Values of $\alpha = 0$ and $\alpha = 1$ for the integration parameter were investigated in this study, as well as explicit (central difference) and implicit (Newmark) time integration schemes for the equations of motion. The results presented in Fig. 2 are for cases where all of these schemes yielded identical results. All solution cases utilized a lumped-mass matrix. Figure 2 indicates that as the value of the fluidity parameter β increases, the viscoplastic solutions approach the rate-independent plasticity response; the linear elastic ($\beta = 0$) and elasto-plastic ($\beta \to \infty$) solutions represent limiting cases of the viscoplastic response. Note that the viscoplastic solution for $\beta = 10000$ s^{-1}

essentially coincides with the elastoplastic response. The solutions of Fig. 2 are in good agreement with those presented previously in Refs. 8 and 13.

Results presented in Fig. 3 compare viscoplastic solutions for β = 10000 s^{-1} obtained from the fully implicit integration parameter (α = 1), the Newmark time integration scheme, and a sequence of increasing time steps. These solutions are compared with the fully explicit (α = 0) result obtained using a time step of Δt_R = 0.45 μs and the central difference time integration scheme. The reference time step Δt_R = 0.45 μs was selected to be slightly below the calculated critical time step Δt_{cr} = 0.5 μs for which the central difference scheme becomes unstable. Here Δt_{cr} is approximated by the ratio d_m/c, where d_m is the smallest element dimension in the mesh and $c = \sqrt{E/\rho}$ the phase velocity of longitudinal waves in a beam. The solutions in Fig. 3 illustrate that, while the fully implicit scheme is unconditionally stable, the accuracy of the solution degenerates with increasing time step size.

3. FINITE-ELEMENT IMPLEMENTATION OF PROPOSED FRACTURE PARAMETERS

3.1 Path-Area Integrals

Two path-area integrals have been incorporated into ADINA for evaluation as potential fracture parameters in crack-arrest studies. For dynamic crack problems formulated in terms of elastoplastic or elastoviscoplastic material models, Atluri et al. [15] have derived the T*-integral to serve as a measure of the intensity of the crack-tip fields. The T*-integral is expressed as an incremental parameter which is evaluated at time step N according to the relations (for the x_1 - coordinate component)

$$T_1^* = \sum_{n=1}^{N} \Delta T_1^* \tag{21}$$

where

$$\Delta T_1^* = \lim_{\varepsilon \to 0} \int_{\Gamma + \Gamma_c} \Delta H_{1j} n_j dS - \int_{V_\Gamma - V_\varepsilon} \Delta H_{1j,j} dV \tag{22}$$

and

$$\Delta H_{1j} = (\Delta W + \Delta K)\delta_{1j} - (\sigma_{ij} + \Delta\sigma_{ij})\Delta u_{i,1} - \Delta\sigma_{ij}\, u_{i,1}, \tag{23}$$

$$\Delta H_{1j,j} = -\Delta\sigma_{ij}(\varepsilon_{ij,1} + \tfrac{1}{2}\Delta\varepsilon_{ij,1}) + \Delta\varepsilon_{ij}(\sigma_{ij,1} + \tfrac{1}{2}\Delta\sigma_{ij,1}) \tag{24}$$

$$- \rho(\ddot{u}_i + \Delta\ddot{u}_i)\Delta u_{i,1} + \rho(\dot{u}_i + \Delta\dot{u}_i)\Delta\dot{u}_{i,1} ,$$

$$- \rho\Delta\ddot{u}_i u_{i,1} + \rho\Delta\dot{u}_i\dot{u}_{i,1} ,$$

$$\Delta W = (\sigma_{ij} + \tfrac{1}{2}\Delta\sigma_{ij})\,\Delta\varepsilon_{ij} , \tag{25}$$

and

$$\Delta K = \rho(\dot{u}_i + \tfrac{1}{2}\Delta\dot{u}_i)\Delta\dot{u}_i . \tag{26}$$

In Eqs. (23) - (26), the terms σ_{ij}, ε_{ij}, u_i, $\dot{u}_i$, $\ddot{u}_i$ represent the components of stress, strain, displacement, velocity and acceleration, respectively, at time step n; the symbol Δ denotes an increment from step n to step n+1. The integrals of Eq. (22) are evaluated on the far-field path Γ, the crack-face path Γ_c, and the enclosed domain $V_\Gamma - V_\varepsilon$ using smoothed nodal stress and strain tensor fields. These smoothed fields are generated from a bilinear least squares mapping [16] of the element Gauss point values to the nodal points of the element. The individual

element contributions to each node are then summed and averaged to give a unique nodal value.

The second path-area integral considered in HSST studies is the $\hat{J}$-integral proposed by Kishimoto et al. [17],

$$\hat{J} = \lim_{\varepsilon \to 0} \; - \int_{\Gamma + \Gamma_c} T_i u_{i,1} dS + \int_{V_\Gamma - V_\varepsilon} \sigma_{ij} \varepsilon_{ij,1} dV + \int_{V_\Gamma - V_\varepsilon} \rho \ddot{u}_i u_{i,1} dV \tag{27}$$

The $\hat{J}$-integral given by Eq. (27) is evaluated using the same smoothing procedure for the stress and strain fields as that described for the T*-integral.

3.2 The Energy Function $\hat{\gamma}$

In the crack-growth modeling techniques employed in ADINA, the element immediately ahead of the crack tip is divided into subelement divisions. During propagation, the tip is moved through these subelements along the crack plane in discrete jumps. The position of the crack tip relative to these subelement divisions is determined from restraining forces which are placed on the crack-plane nodes of the element adjacent to the crack tip (see Fig. 4); these forces are released incrementally as the tip propagates through the element. The restraining forces are postulated to vary with the crack-tip location according to the relation

$$\frac{F_i}{F_{oi}} = [1 - a(t)/\Delta X]^R \quad , \tag{28}$$

where F_i is the force at node "i", F_{oi} is the force at node "i" just prior to node release, and "a" is the length of the crack in the element of length ΔX. In HSST studies, the exponent in Eq. (28) has been assigned the values R = 0.5, 1.0, and 1.5.

Following Brickstad [8], the energy flow to the crack-tip region per unit area of crack extension, $\hat{\gamma}$, is approximated by calculating the work performed by the forces F_i (i = 1,2) according to the relation

$$\hat{\gamma} = \frac{2}{h \cdot \Delta X} \sum_{i=1}^{2} \int_{t'}^{t' + \overline{\Delta t}} [F_i(t)\, \dot{u}_i(t)]dt \quad . \tag{29}$$

In Eq. (29), h denotes the thickness of the plate, $\overline{\Delta t}$ the time interval required for the crack-tip to traverse the element of length ΔX, t' the initial time for release of the element, and $\dot{u}_i$ the velocity component of node "i" normal to the crack plane. When conditions of LEFM pertain, the function $\hat{\gamma}$ represents an approximation of the strain energy release rate.

4. APPLICATIONS TO DYNAMIC FRACTURE STUDIES

The predictive capabilities of the nonlinear techniques described in the previous sections are being evaluated through applications of ADINA to analyses of HSST wide-plate crack-arrest experiments. In the following, the program is applied to one specific wide-plate test (WP-1.2) from the HSST WP-1 series [1].

4.1 Viscoplastic-Dynamic Analysis of a Wide-Plate Experiment

The SEN plate specimen (1 × 1 × 0.1 m) used in wide-plate test WP-1.2 [1] is shown schematically in Fig. 5. The plate was cooled on the

notched edge and heated on the other edge to give a linear temperature gradient (T_{min} = -97°C, T_{max} = 207°C) along the plane of crack propagation. Upon initiating propagation of the crack in cleavage, arrest was intended to occur in the higher-temperature ductile region of the specimen. The specimen had an initial crack depth-to-plate width ratio (a/w) of 0.2. The specimen was welded to pull-plates which have a pin-to-pin length of 9.6 m to minimize stress wave effects. Material properties of the wide-plate material are described in Ref. 1.

The two-dimensional (2-D) plane stress finite element model of one-half of the wide-plate configuration used in the analyses and depicted in Fig. 6 consists of 2377 nodes and 715 eight-noded isoparametric elements. The exponent in the node release function [Eq. (28)] was set at R = 1.0 for elastic and R = 1.5 for viscoplastic material models. For the dynamic analyses, the applied load was fixed at the value that prevailed at crack initiation (F_{in} = 18.9 MN). The Gauss point rule selected for integration of the finite element model was 2 × 2 for the stiffness matrix and 3 × 3 for the consistent mass matrix. The time step was set at Δt = 4 μs for the elastodynamic analyses and at Δt = 2 μs for the viscoplastic dynamic analyses; the Newmark time integration scheme was used for all cases. For the viscoplastic analyses, the Bodner-Parton equations summarized in Tables 1 and 2 were integrated using the parameter α = 1; global equilibrium interations were performed during each time step.

Generation-mode analyses of test WP-1.2 were performed using the estimate of crack position vs. time [Fig. 7(a)] constructed in part from strain-gage data recorded at the crack-line strain-gage locations in

Fig. 5. (In a generation-mode analysis, the crack-tip is propagated incrementally according to a prescribed crack position vs time relation.) Figure 7(a) shows the two measured crack arrests at a_{fm1} = 0.55 m and at a_{fm2} = 0.65 m which occurred at times t_{m1} = 0.96 ms and at t_{m2} = 2.7 ms after crack initiation, respectively. Results from viscoplastic analyses of the first 3 ms of the dynamic event using the Bodner-Partom model are presented in Figs. 7(b) - (c). The interval of crack arrest beginning at time t ≈ 1 ms [Fig. 7(a)] coincides with a sharp drop in the maximum effective viscoplastic strain rate [Fig. 7(b)]. In Fig. 7(c), the time histories of the functions T*, $\hat{J}$, and $\hat{\gamma}$ are expressed in terms of pseudo-K_I values ($K_I = \sqrt{ET^*}$, E = 206.9 GPa) for purposes of comparison with elastodynamic values. The results given in Fig. 7(c) indicate generally good agreement between the functions T*, $\hat{J}$, and $\hat{\gamma}$; for both the elastic and inelastic cases, the T* and $\hat{J}$ calculations coincide. The difference in energy flow to the crack tip region in the viscoplastic case is due primarily to dissipation processes occurring in the developing plastic zone around the propagating crack tip. When the viscoplastic analysis was repeated using the Perzyna model summarized in Tables 3 and 4, the resulting time histories of the fracture parameters were not significantly different from the Bodner-Partom values in Fig. 7(c).

4.2 Model-Dependent Effects in Viscoplastic Fracture Analysis

Results obtained thus far from viscoplastic-dynamic fracture analyses of HSST wide-plate tests exhibit a significant dependence on finite element mesh refinement. Figure 8 compares results from generation-mode viscoplastic analyses of wide-plate test WP-1.2 obtained from models

having different mesh refinements along the crack plane. The results are expressed in terms of pseudo-K_I values computed from the rate-of-work function $\hat{\gamma}$ [Eq. (29)] and plotted vs. crack length for the first run-arrest event. The characteristic mesh size is defined as the ratio of the crack-path element width to the plate width. The ORNL analysis results shown in Fig. 8 for mesh sizes 1/22, 1/40 and 1/50 were obtained from ADINA analyses described in Refs. 18 and 9 and in the previous section of this paper, respectively. Also shown in Fig. 8 are results obtained by Brickstad [14] using mesh sizes 1/40 and 1/80 and the Perzyna viscoplastic model described in Tables 3 and 4. These combined results indicate that the dynamic viscoplastic solutions of the wide-plate test expressed in terms of the parameters T*, $\hat{J}$, and $\hat{\gamma}$ have not yet converged for the mesh refinements employed thus far in these studies.

Insight into the difficulties associated with modeling rapid crack propagation events in RPV steels exhibiting viscoplastic behavior are provided by two recent studies. Sheu [19] studied the mode-I plane strain problem of dynamic steady-state crack growth in A533B steel using the Bodner-Partom model summarized in Tables 1 and 2 of this paper and the assumption of small-scale yielding. Focusing on the immediate area surrounding the elastic-plastic boundary, Sheu [19] resolved the near crack-tip singular fields using a finite element model with element dimensions approximately 0.1% of the elastic-plastic zone size. (For the Bodner-Partom model, the stress field is $r^{-1/2}$ singular and the elastic strain rates dominate the plastic strain rates near the crack tip.) Popelar [20] has elaborated further on the study of Sheu [19] by

showing that the zone of dominance becomes smaller for increasing values of the limiting plastic strain rate, Do, and is approximately 0.1% of the plastic zone size for Do = 10^8 s^{-1}. Furthermore, for A533B steel over a temperature range from -60 to 100°C and a crack speed of one-half the Rayleigh wave speed, Popelar [20] estimates that the zone of dominance extends from ~5 to 55 μm compared to an inelastic region with dimensions 0.1 to 15 mm. Given that the computational capacity were available to resolve such a small region using finite elements, it is clear that elements of this size invade the micro-heterogeneity of the material and broach the limits of isotropic continuum analysis.

Several techniques are being explored to circumvent these stringent requirements on crack-tip mesh refinement and related difficulties associated with possible violations of continuum assumptions. Nishioka [21] has proposed an exclusion zone technique that obviates the need for highly-refined crack-tip elements. In this technique, a small rectangular domain of height 2ε is defined around the crack tip to approximate a finite fracture process zone. During the dynamic analysis, this rectangle is extended in length (but not in height) to include a portion of the plastic wake behind the advancing crack. Nishioka [21] advocates excluding the integration of a portion of the volume term of the T*-integral [see Eq. (22)] from this extending exclusion zone. According to a study by Nishioka [21], the T*-integral should be essentially invariant with respect to the size of this extending domain provided ε is sufficiently small. To investigate the potential of the foregoing technique for characterizing fracture behavior, O'Donoghue [22] has performed studies of the geometry independence of the two-component

parameter (T^*, ε) using a center-cracked panel problem. Results of these analyses indicate that the time history of T^* is relatively insensitive to mesh refinement for a given height of the exclusion zone. Based on these preliminary calculations, further studies will be conducted in the HSST program on the geometry independence of the (T^*, ε) parameter when applied to small- and large-specimen crack run-arrest data.

Moving singular-element formulations represent an alternative technique for achieving convergent fracture parameter solutions in the context of viscoplastic-dynamic fracture analysis. A review of the various computational methods that have employed singular elements in elastodynamic fracture applications is given by Nishioka and Atluri [23]. Two aspects associated with moving singular-element formulations may improve convergence characteristics in inelastic fracture applications. The first is the influence of including singular functions in the solution space of the Ritz-Galerkin approximation. The second, possibly more subtle aspect, is the capability of maintaining a node positioned precisely at the moving discontinuity. (Current nodal-relaxation techniques do not specify the exact position of the crack tip except when the tip is located at an interelement boundary.) In preliminary work, Thesken and Gudmundsson [24] have implemented a variable-order singular element proposed by Akin [25] into an elastodynamic finite-element formulation and have illustrated its advantages in modeling stationary cracks subjected to dynamic loading. More recently, Thesken and Gudmundsson [26] have incorporated a moving element formulation which allows an adjustable region of convecting elements (including the

variable-order singular element) to be embedded at the crack tip within a finite body. The latter technique permits the order of the crack-tip singularity to be specified by a variable parameter for dynamic crack growth problems. This technique has shown good agreement with known analytic elastodynamic solutions. Work is currently under way in the HSST Program to update the moving element formulation to accommodate viscoplastic material behavior. The resultant formulation will be investigated for its potential in resolving the near crack-tip singular fields of the Bodner-Partom constitutive model while remaining in the size regime of a continuum element.

5. CONCLUSION

This paper has described a portion of the HSST crack-arrest studies wherein various viscoplastic constitutive models and several proposed nonlinear fracture criteria were installed in the ORNL version of the ADINA finite element computer program. Modifications implemented in ADINA allow integration of the viscoplastic constitutive equations using the effective stress function algorithm of Kojic and Bathe [5]. The modified formulation was found to be effective in applications to viscoplastic dynamic problems that utilize the Bodner-Partom and the Perzyna constitutive models.

The capabilities of the nonlinear fracture techniques installed in ADINA were evaluated through applications to the HSST wide-plate crack-arrest experiment WP-1.2. Results from generation-mode viscoplastic-dynamic fracture analyses of the WP-1.2 experiment indicated good agreement among the fracture parameters T^*, $\hat{J}$ and $\hat{\gamma}$. Apparently, it is sufficient to focus on the T^*-integral in future studies as representative of this class of energy-based fracture parameters.

Viscoplastic-dynamic fracture analyses of the wide-plate tests, when expressed in terms of the fracture parameters (T*, etc.), exhibited a strong dependence on mesh refinement. These results, combined with asymptotic studies by Sheu [19] and Popelar [20], indicate that resolution of the crack-tip singular fields in viscoplastic models of engineering structures using conventional finite element formulations is apparently not within reach currently for practical mesh sizes, even in a super-computer environment. Alternative techniques are being investigated that include a two-component parameter (T*, ε) to exclude the high-strain-rate region from a portion of the calculations and a moving variable-order singular element formulation to build the crack-tip singularity into the finite element approximation.

References

1. D. J. Naus et al., *Crack Arrest Behavior in SEN Wide Plates of Quenched and Tempered A533B Steel Tested under Nonisothermal Conditions*, NUREG/CR-4930 (ORNL-6388), Martin Marietta Energy Systems, Inc., Oak Ridge Natl. Lab., September 1987.

2. B. R. Bass et al., "Fracture Analyses of Heavy-Section Steel Technology Wide-Plate Crack-Arrest Experiments," *Fracture Mechanics: Nineteenth Symposium*, ASTM STP-969, T. A. Cruse (Ed.)., pp. 691-733 (1987).

3. C. E. Pugh et al., "Crack Run-Arrest Behavior in Wide SEN Plates of a LWR Pressure Vessel Material," Vol. G, *Transactions of the 9th International Conference on Structural Mechanics in Reactor Technology, Lausanne, Switzerland, Aug. 17-21, 1987*, pp. 21-26.

4. K. J. Bathe, *ADINA - A Finite Element Program for Automatic Dynamic Incremental Nonlinear Analysis*, Report AE 84-1, Massachusetts Institute of Technology, Cambridge, MA (December 1984).

5. M. Kojic and K. J. Bathe, "The Effective-Stress-Function Algorithm for Thermo-Elasto-Plasticity and Creep," *Int. J. Numer. Meth. Engng.*, Vol. 24, No. 8, pp. 1509-1532 (1987).

6. M. F. Kanninen and C. H. Popular, *Advanced Fracture Mechanics*, Oxford University Press, New York, 1985, pp. 214-230.

7. L. Dahlberg et al., "Influence of Specimen Geometry on Crack Propagation and Arrest Toughness," *Crack Arrest Methodology and Applications*, ASTM STP-711, G. T. Hahn and M. F. Kanninen (Eds), pp. 89-108 (1980).

8. B. Brickstad, "A Viscoplastic Analysis of Rapid Crack Propagation Experiments in Steel," *J. Mech. Phys. Solids*, Vol. 31, pp. 307-27 (1983).

9. B. R. Bass et al., "Late-Event Viscoplasticity in Wide-Plate Crack Arrest Test," *Int. J. Pres. Ves. and Piping*, Vol. 31, pp. 325-348 (1988).

10. S. R. Bodner and Y. Partom, "Constitutive Equations for Elastic Viscoplastic Strain Hardening Materials," *J. Appl. Mech.*, Vol. 42, p. 385 (1975).

11. P. Perzyna, "Fundamental Problems in Visco-Plasticity," pp. 244-368 in *Recent Advances in Applied Mechanics*, Academic Press, New York, 1966.

12. M. F. Kanninen et al., "Viscoplastic Characterization of A533B Steel," in *Heavy-Section Steel Technology Program Semiann. Prog. Rep. April-September 1986*, NUREG/CR-4219, Vol. 3, No. 2 (ORNL/TM-9593/V3&N2), Martin Marietta Energy Systems, Inc., Oak Ridge Natl. Lab., December 1986.

13. S. K. Thakkar and K. G. Stagg, "Nonlinear Dynamic Analysis of Stress-Wave Propagation Problems," *Proceedings of First International Conference on Nonlinear Problems*, Pineridge Press, Swansea, pp. 937-958 (1980).

14. B. Brickstad, "Wide-Plate Analysis of WP-1.2 and WP-1.5", *Third Annual HSST Workshop on Crack Arrest Technology*, National Bureau of Standards, Gaithersburg, MD, May 1987.

15. S. N. Atluri, T. Nishioka, and M. Nakagaki, "Incremental Path Independent Integrals in Inelastic and Dynamic Fracture Mechanics" *Eng. Fract. Mech.*, Vol. 20-2, pp. 209-244 (1984).

16. E. Hinton and J. S. Campbell, "Local and Global Smoothing of Discontinuous Finite Element Functions Using a Least Squares Method," *Int. J. Numer. Meth. Engng.*, Vol. 8, pp. 461-480 (1974).

17. K. Kishimoto, S. Aoki, and M. Sakata, "On the Path-Independent Integral - $\hat{J}$," *Eng. Fract. Mech.*, Vol. 13, pp. 841-50 (1980).

18. B. R. Bass et al., "Evaluation of Viscoplastic Fracture Criteria and Analysis Methods," *Proc. of U.S. Nuclear Regulatory Commission Fifteenth Water Reactor Safety Information Meeting*, National Bureau of Standards, Gaithersburg, Maryland, NUREG/CP-0091, 52-91, 1988.

19. Y. C. Sheu, "Dynamic Elastic-Viscoplastic Crack Growth," Ph.D. Dissertation, School of Engineering, Ohio State University, 1988.

20. C. H. Popelar, "A Viscoplastic Analysis for Predicting the Dynamic Fracture Toughness of A533B Steel," submitted for publication.

21. T. Nishioka, "Finite Element Analysis of the T*-Integral in Nonlinear Dynamic Fracture Problems," Proceedings of International Conference on Computational Engineering Science, April 10-14, 1988, Atlanta, GA, 9.V.1-4 (1988).

22. P. O'Donoghue, "Crack-tip Characterizing Parameters in Dynamic Viscoplstic Fracture Mechanics", *Fourth Annual HSST Program Workshop on Dynamic Fracture and Crack Arrest Technology*, National Bureau of Standards, Gaithersburg, MD., June 1988.

23. T. Nishioka and S. N. Atluri, "Computational Methods in Dynamic Fracture," in *Computational Methods in the Mechanics of Fracture*, (Ed.) S. N. Atluri, North Holland, Amsterdam (1986).

24. J. C. Thesken and P. Gudmundsson, "Application of a Variable Order Singular Element to Dynamic Fracture Mechanics," *Computational Mechanics*, Vol. 2, pp. 307-316 (1987).

25. J. E. Akin, "The Generation of Elements with Singularities," *Int. J. Numer. Meth. Engng.*, Vol. 10, pp. 1249-1259 (1976).

26. J. C. Thesken and P. Gudmundsson, "Application of a Moving Variable Order Singular Element to Dynamic Fracture Mechanics," to be published.

Table 1. Summary of relations for the Bodner-Partom constitutive model with isotropic hardening and without thermal recovery

---

1. Flow Law:

$$\dot{e}_{ij} = \dot{e}_{ij}^{e} + \dot{e}_{ij}^{p}$$

$$\dot{e}_{ij}^{p} = \lambda S_{ij}; \quad \dot{e}_{kk}^{p} = 0$$

with $$S_{ij} = \sigma_{ij} - \frac{1}{3}\delta_{ij}\sigma_{kk}$$

2. Kinetic Equation:

$$D_2^{p} = D_o^{2} \exp\left[-\left(\frac{Z^2}{3J_2}\right)^{n}\right]$$

with $$Z = Z^{I}$$

$$D_2^{p} = \frac{1}{2}\dot{e}_{ij}^{p}\dot{e}_{ij}^{p}$$

$$J_2 = \frac{1}{2}S_{ij}S_{ij}$$

$$\lambda^2 = D_2^{p}/J_2$$

3. Evolution Equation of Isotropic Hardening Internal Variable:

$$\dot{Z}^{I} = m_1(Z_1 - Z^{I})\dot{W}_p$$

with $$Z^{I}(0) = Z_o; \quad \dot{W}_p = S_{ij}\dot{e}_{ij}^{p}; \quad W_p(0) = 0$$

4. Material Constants:

$$D_o,\ Z_o,\ Z_1,\ m_1,\ n, \text{ and elastic constants}$$

Table 2. Constants for the Bodner-Partom constitutive model representation for A533 grade B class 1 steel

$D_o = 10^8\ s^{-1}$, $m_1 = .059\ MPa^{-1}$

Temperature (°C)	n	Z_o (MPa)	Z_1 (MPa)
-60	1.62	1772	2224
-10	1.68	1491	1992
50	1.75	1379	1804
65	1.93	1223	1616
85	2.23	1035	1390
100	2.57	907	1236
175	2.77	827	1112

Table 3. Summary of relations for the Perzyna constitutive model with linear strain hardening

1. Flow Law:

$$\dot{e}_{ij} = \dot{e}^{e}_{ij} + \dot{e}^{p}_{ij}$$

$$\dot{e}^{p}_{ij} = \begin{cases} \beta\phi(\bar{\sigma}) \dfrac{\sqrt{3}}{2\sqrt{J_2}} S_{ij} & \text{if } \bar{\sigma} > \bar{\sigma}_o \\ 0 & \text{if } \bar{\sigma} \leq \bar{\sigma}_o \end{cases}$$

with $S_{ij} = \sigma_{ij} - \frac{1}{3}\delta_{ij}\sigma_{kk}$

$$\phi(\bar{\sigma}) = \left(\frac{\bar{\sigma} - \bar{\sigma}_o}{\bar{\sigma}_o}\right)^N$$

$$\bar{\sigma} = (3\ J_2)^{1/2}$$

$$J_2 = \frac{1}{2} S_{ij} S_{ij}$$

$$\bar{\sigma}_o = \sigma_{yI} + H' \bar{e}^{\,p}$$

σ_{yI} = initial yield stress in uniaxial tension

$\bar{e}^{\,p}$ = accumulated effective plastic strain

2. Material Constants:

β, N, H' and elastic constants

Table 4. Constants for the Perzyna constitutive model representation of A533 grade B class 1 steel

$N = 2.5$
$\beta = 10000\ (s^{-1})$
$E = 2.0684$ (GPa)
$E_T = E/75$ (linear strain hardening)
$H' = E\ E_T/(E + E_T)$
$\sigma_{yI} = 449 - 0.3535\ T$ (MPa) where units of T are deg C.

Figure Captions

Fig. 1. Comparison of Bodner-Partom constitutive model with measured stress-strain data for A533 grade B class 1 steel at a temperature of 100°C and strain rates of 550 s^{-1} and 0.001 s^{-1}.

Fig. 2. Variation of response with fluidity parameter for clamped beam subjected to a suddenly applied load.

Fig. 3. Variation of response with time step size for clamped beam subjected to a suddenly applied load.

Fig. 4. Crack-propagation model for calculation of $\hat{\gamma}$.

Fig. 5. Wide-plate assembly and crack-arrest specimen: (a) pull-plate assembly; (b) specimen with strain-gage locations.

Fig. 6. Finite element model of wide-plate assembly.

Fig. 7. Time histories of crack-depth ratio, maximum effective viscoplastic strain rate, and fracture parameters from analysis of wide-plate test WP-1.2. (a) Crack-depth ratio, (b) maximum effective viscoplastic strain rate, (c) fracture parameters.

Fig. 8. Comparison of results [$K_I(\hat{\gamma})$ vs crack depth] from generation-mode viscoplastic-dynamic analyses of test WP-1.2 for four crack path mesh refinements.

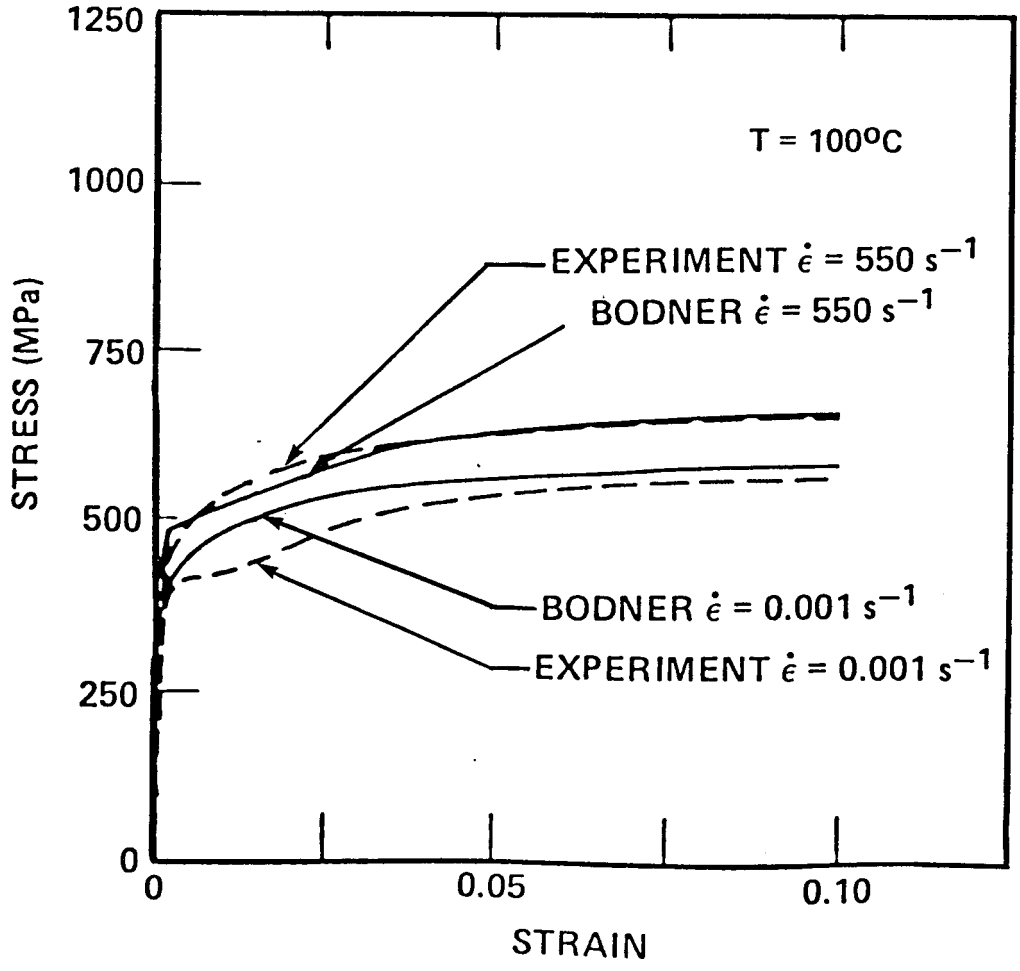
1250
1000
750
500
250
0
STRESS (MPa)
T = 100°C
EXPERIMENT $\dot{\epsilon}$ = 550 s^{-1}
BODNER $\dot{\epsilon}$ = 550 s^{-1}
BODNER $\dot{\epsilon}$ = 0.001 s^{-1}
EXPERIMENT $\dot{\epsilon}$ = 0.001 s^{-1}
0
0.05
0.10
STRAIN

ornl

Fig 1

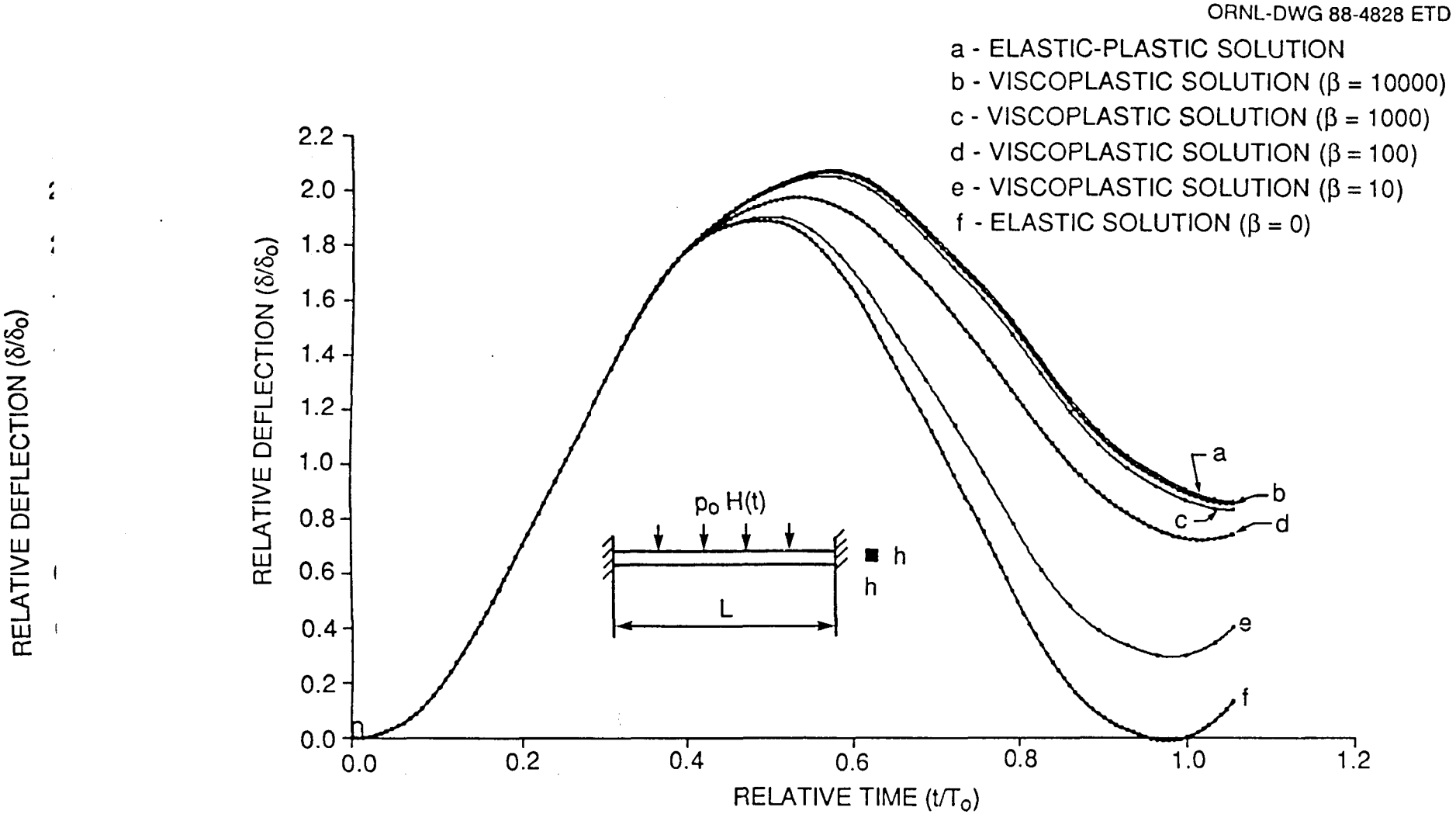
ORNL-DWG 88-4828 ETD
a - ELASTIC-PLASTIC SOLUTION
b - VISCOPLASTIC SOLUTION (β = 10000)
c - VISCOPLASTIC SOLUTION (β = 1000)
d - VISCOPLASTIC SOLUTION (β = 100)
e - VISCOPLASTIC SOLUTION (β = 10)
f - ELASTIC SOLUTION (β = 0)
RELATIVE DEFLECTION (δ/δo)
RELATIVE TIME (t/To)
0.0
0.2
0.4
0.6
0.8
1.0
1.2
1.4
1.6
1.8
2.0
2.2
po H(t)
h
h
L
a
b
c
d
e
f

Fig 2

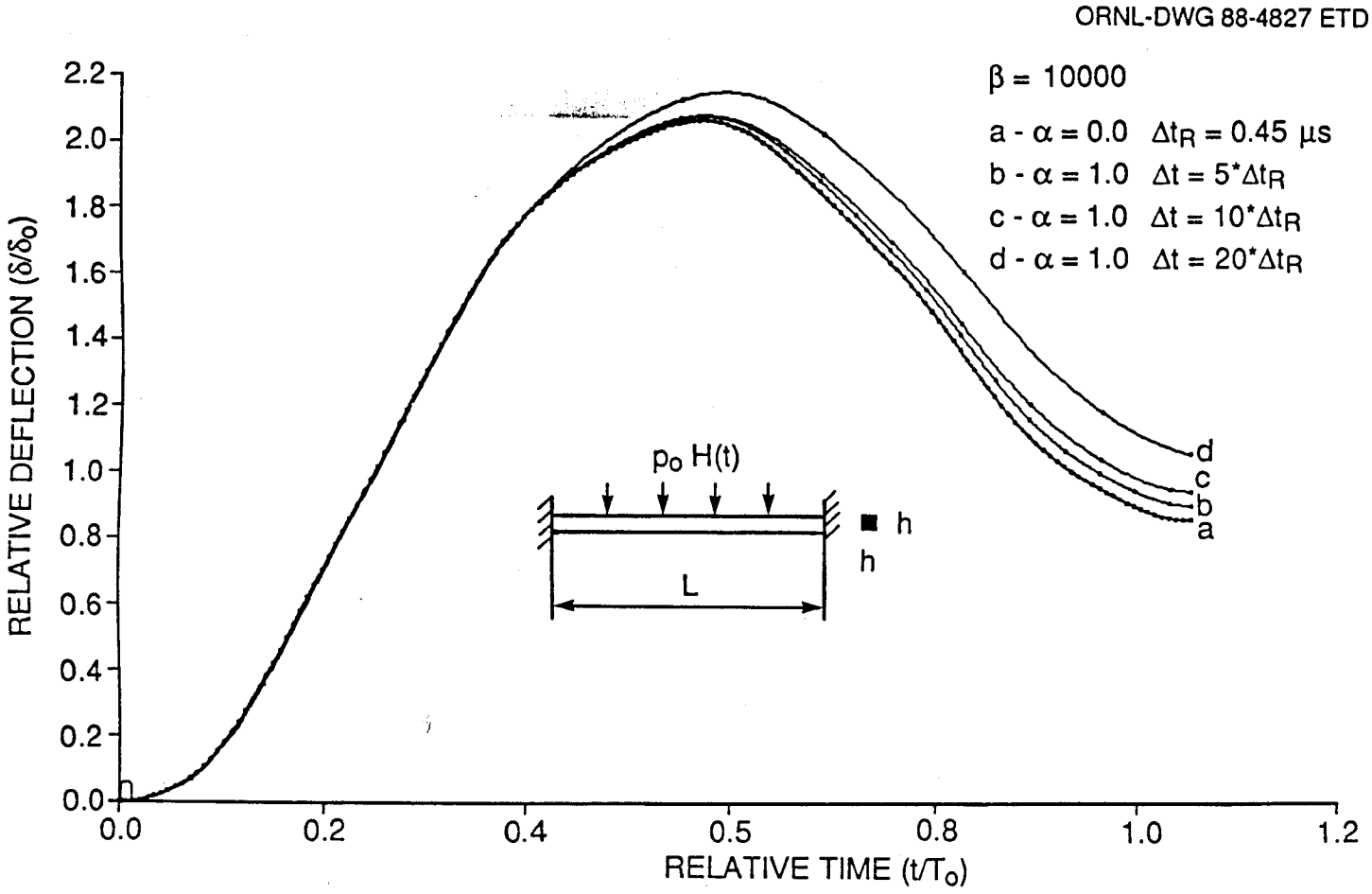
ORNL-DWG 88-4827 ETD
β = 10000
a - α = 0.0 Δt_R = 0.45 μs
b - α = 1.0 Δt = 5*Δt_R
c - α = 1.0 Δt = 10*Δt_R
d - α = 1.0 Δt = 20*Δt_R
RELATIVE DEFLECTION (δ/δ_o)
RELATIVE TIME (t/T_o)
2.2
2.0
1.8
1.6
1.4
1.2
1.0
0.8
0.6
0.4
0.2
0.0
0.0
0.2
0.4
0.5
0.8
1.0
1.2
p_o H(t)
h
h
L
a
b
c
d

Fig. 3

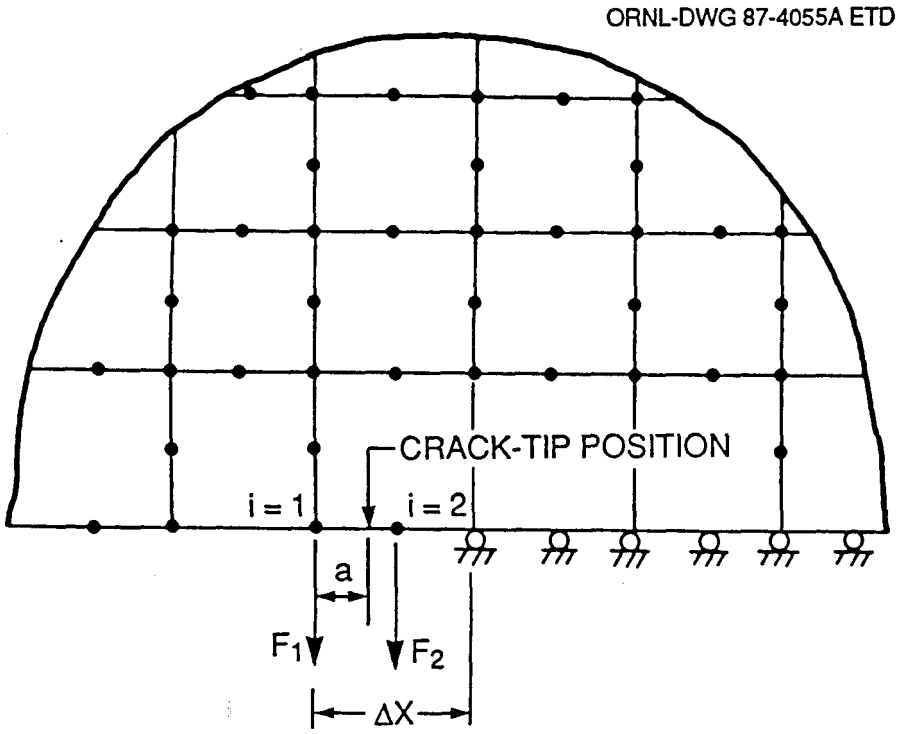

Fig. 4

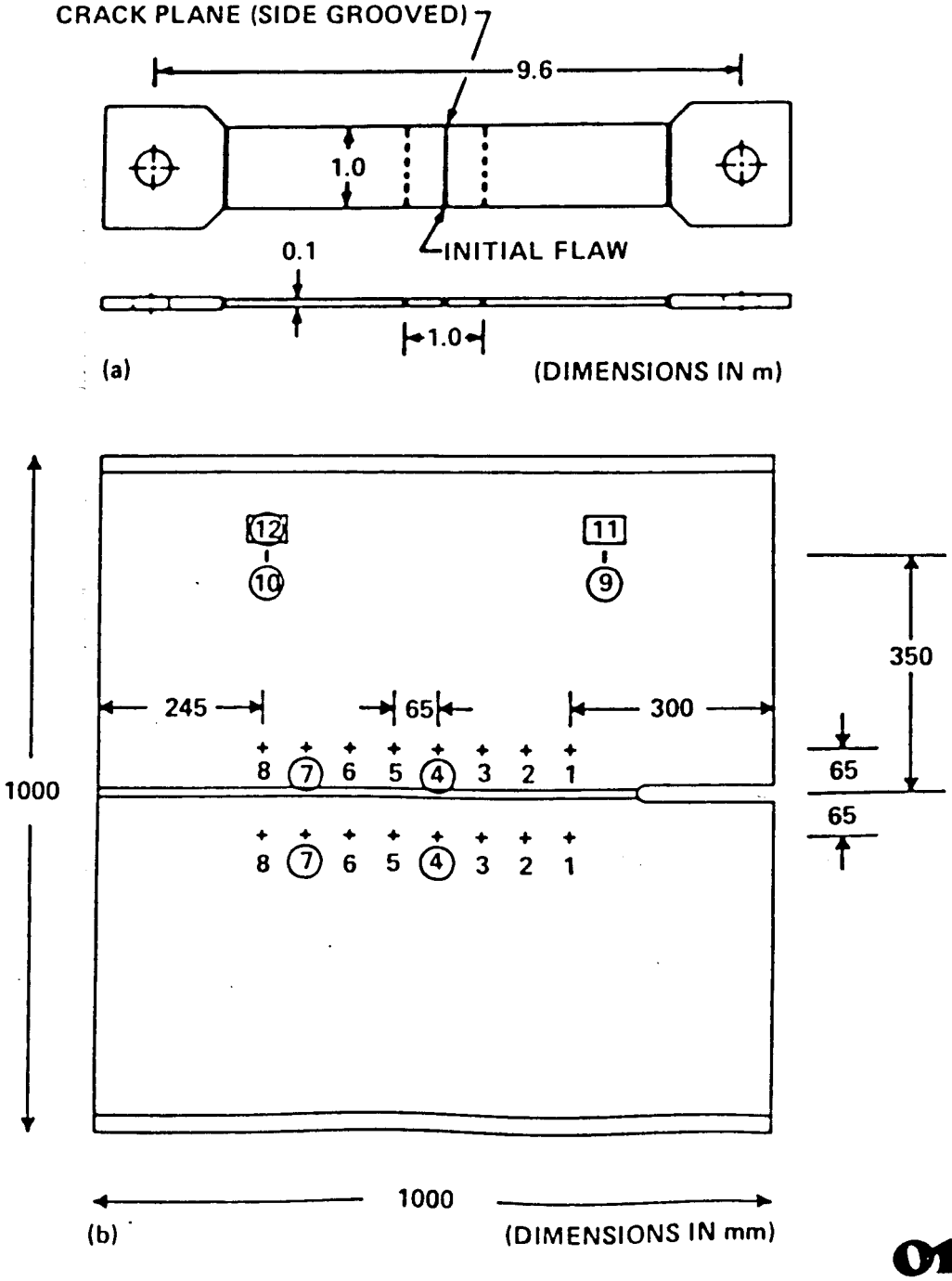
CRACK PLANE (SIDE GROOVED)
9.6
1.0
0.1
INITIAL FLAW
1.0
(a)
(DIMENSIONS IN m)
12
11
10
9
350
245
65
300
8 7 6 5 4 3 2 1
65
1000
65
8 7 6 5 4 3 2 1
1000
(b)
(DIMENSIONS IN mm)

ornl

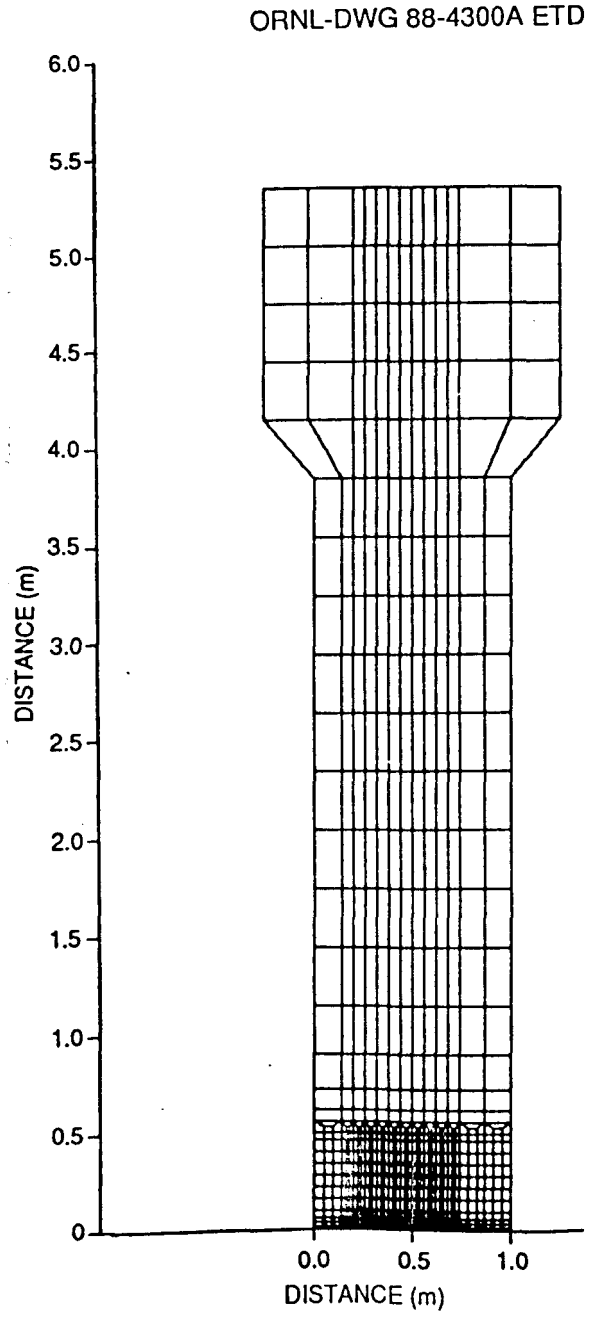
ORNL-DWG 88-4300A ETD
6.0
5.5
5.0
4.5
4.0
3.5
3.0
2.5
2.0
1.5
1.0
0.5
0
DISTANCE (m)
0.0
0.5
1.0
DISTANCE (m)

Fig 6

ORNL-DWG 88-4302A ETD

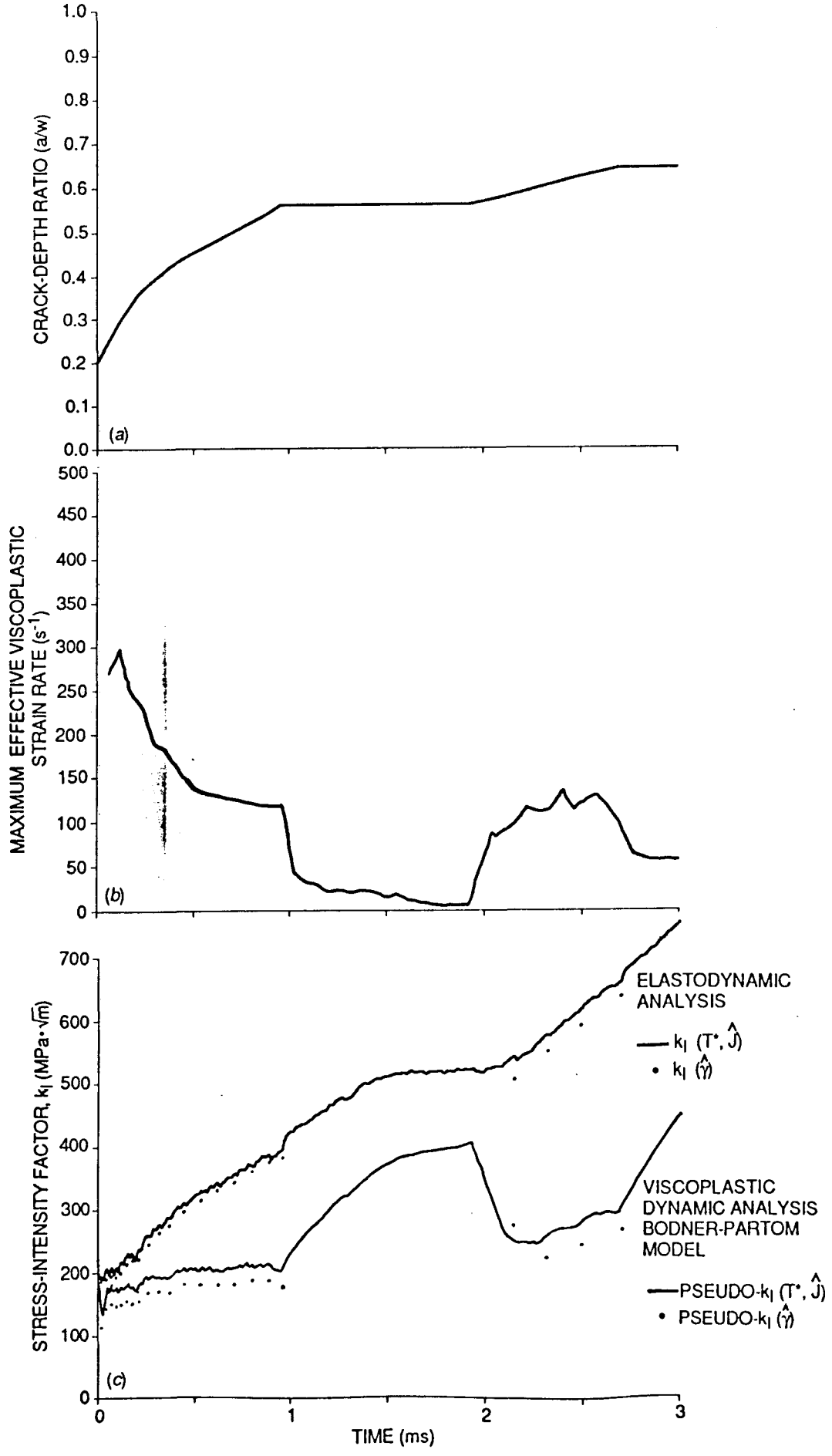

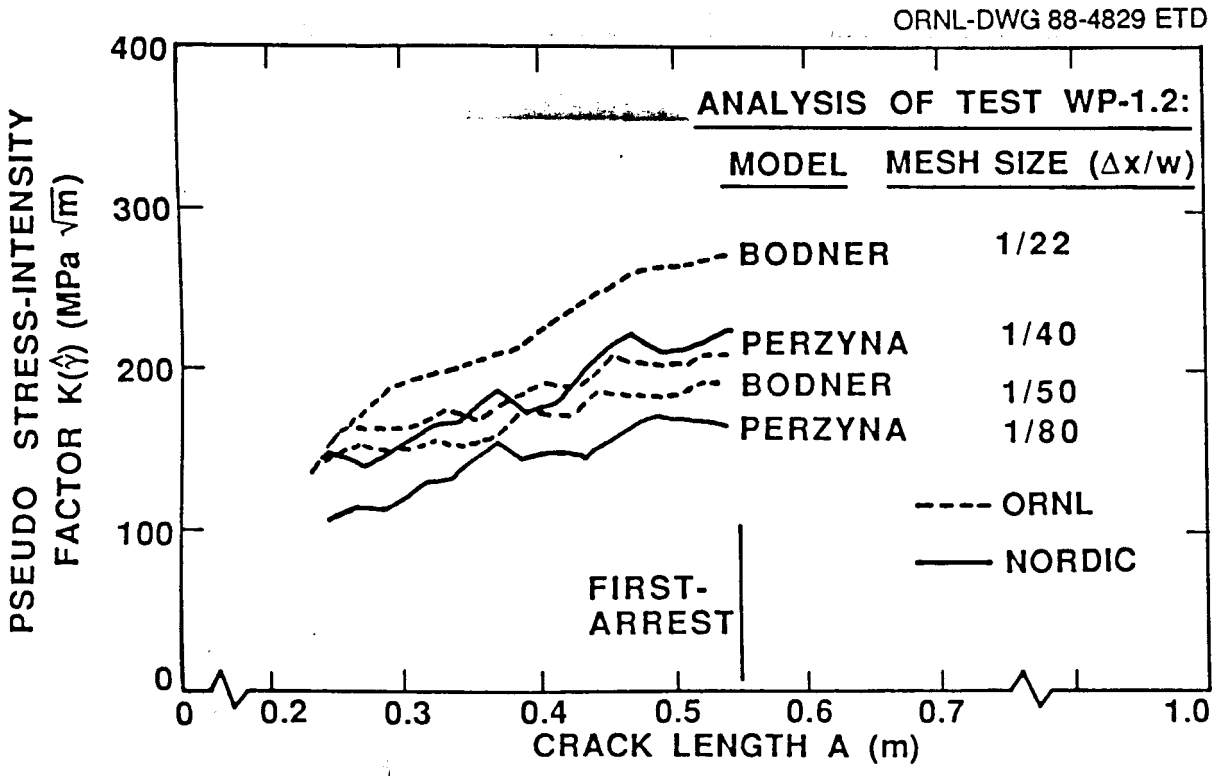
ORNL-DWG 88-4829 ETD
ANALYSIS OF TEST WP-1.2:
MODEL
MESH SIZE (Δx/w)
BODNER 1/22
PERZYNA 1/40
BODNER 1/50
PERZYNA 1/80
ORNL
NORDIC
FIRST-ARREST
PSEUDO STRESS-INTENSITY FACTOR K(γ̇) (MPa √m)
CRACK LENGTH A (m)
400
300
200
100
0
0
0.2
0.3
0.4
0.5
0.6
0.7
1.0

Fig. 8